Dynamic and Thermodynamic Processes Related to Sea-Ice Surface Melt Advance in the Laptev Sea and East Siberian Sea

Hongjie LIANG, [1] Wen ZHOU [1,2]

[1] Department of Atmospheric and Oceanic Sciences & Institute of Atmospheric Sciences, Fudan University, Shanghai, China

[2] Center for Polar Ice & Snow and Climate Change Research, Polar Research Institute of China, Shanghai, China

Correspondence to: Wen Zhou (wen_zhou@fudan.edu.cn)

Aug, 2023

17 ABSTRACT

18   Arctic summer sea ice has shrunk considerably in recent decades. This study

19 investigates springtime sea-ice surface melt onset in the Laptev Sea and East Siberian

20 Sea, which are key seas along the Northeast Passage. Instead of region-mean melt onset,

21 we define an index of Melt Advance, which is the areal percentage of a sea that has

22 experienced sea-ice surface melting before the end of May. Four representative

23 scenarios of Melt Advance in the region are identified. Each scenario is accompanied

24 by a combination of distinct patterns between atmospheric circulation, atmospheric

25 thermodynamic state, sea ice cover (polynya activity), and surface energy balance in

26 May. In general, concurrent with faster Melt Advance are warmer and wetter

27 atmosphere, less sea ice cover, and surface energy gains in spring. Melt Advance can

28 be potentially used in the practical seasonal prediction of summer sea ice cover. This

29 study implicates the interannual and interdecadal flexibility of spring circulation in the

30 lower troposphere and the significance of seasonal evolution in the Arctic.

31

32

1. Introduction

34   Since the 1970s, satellites have enabled global detection of the Earth. Arctic

35 summer sea ice extent is found to have decreased dramatically in the past four decades

36 (Petty et al., 2020; Stroeve and Notz, 2018), which is a prominent indicator of global

37 warming. In fact, the Arctic has a faster warming trend than elsewhere on the planet,

38 especially in the lower troposphere during the cold season(Cohen et al., 2014; Serreze

39 et al., 2009; Screen and Simmonds, 2010). This phenomenon, called Arctic

40 Amplification, presumably results from reduced sea ice cover and enhanced oceanic

41 energy release toward the atmosphere, atmospheric and oceanic heat transport from

42 lower latitudes, and local positive feedbacks (Serreze et al., 2009; Cohen et al., 2014;

43 Taylor et al., 2022). Some research has indicated that the mid-latitudes may frequently

44 experience severe winters due to the Arctic Amplification which reduces the meridional

45   temperature gradient and in turn amplifies the planetary Rossby wave and makes it

46   more stationary (Francis and Vavrus, 2015). In the Arctic, positive ice-albedo feedback

47   is active in the melt season (Budyko, 1969; Kashiwase et al., 2017; Sellers, 1969): after

48   sea ice begins to melt in spring, surface albedo decreases substantially, which favors

49   more solar radiation absorption and promotes further sea ice melting. Based on this

50   notion, some studies have tried to predict Arctic summer sea ice cover by sea-ice surface

51   Melt Onset (MO) in spring, i.e., the date when the sea ice surface begins to form liquid

52   water (Petty et al., 2017; Wang et al., 2011). Currently, satellite remote sensing helps

53   us construct the pan-Arctic sea ice MO, which is not possible with only in-situ field

54   observations. However, for sea ice lateral and bottom melting, satellites are less useful

55   and buoys are widely employed (Lei et al., 2022).

56   Many studies have touched on sea ice MO in springtime (Drobot and Anderson,

57   2001; Bliss and Anderson, 2014; Horvath et al., 2021; Crawford et al., 2018; Markus et

58   al., 2009; Stroeve et al., 2014). Generally, sea ice MO is becoming earlier in most parts

59   of the Arctic, which is consistent with the Arctic warming. Another notable feature of

60   MO is its regionality. For example, the Barents Sea, Kara Sea, Laptev Sea, and East

61   Siberian Sea are around the same latitudes along the Siberian coast, but the MO trends

62   were -7.1, -5.2, -2.8, and -1.8 days per decade from 1979 to 2013, respectively (Stroeve

63   et al., 2014). Liang and Su (2021) investigated the interannual early/late relationship of

64   MO between the Laptev Sea and East Siberian Sea, which is related to the large-scale

65   atmospheric pattern of the Barents Oscillation (Skeie, 2000). Locally, synoptic

66   processes are regarded as responsible for interannual variability. Mortin et al. (2016)

67   argued that sea ice MO is generally associated with higher surface air temperature

68   (SAT), total-column water vapor (TWV), and cloud cover, which promotes downward

69   longwave radiation.

70   The Laptev Sea (LS) and East Siberian Sea (ESS) are marginal seas of the Arctic

71   Ocean, north of Siberia along the Northeast Passage (Fig. S1). The longitude-latitude

72   ranges are around 70°N-80°N and 100°E-180°, covering 0.66 and 1.14 million km^2 for

73 the LS and ESS, respectively. These two seas are among the regions where sea ice

74 decline in September during the past four decades has been the most prominent, and

75 they are key regions for safe transportation across the Northeast Passage. In spring, sea

76 ice almost completely covers the seas, while in summer, sea ice substantially retreats

77 off the coast.

78   Focusing on the LS and ESS, which usually have the most persistent sea ice

79 coverage in the Northeast Passage, this study aims to demonstrate the springtime

80 processes related to different Melt Advance scenarios and explore the linkage between

81 springtime Melt Advance and summertime sea ice coverage.

82

83

84 **2. Data and Methods**

85   Sea ice Melt Onset (MO) is the date when the sea ice surface begins to melt in

86 spring, which is retrieved from satellite passive microwave signals (Markus et al., 2009).

87 Liquid water has greater emissivity than ice/snow, so surface melting invokes changes

88 in passive microwave signals. The dataset is distributed by the National Aeronautics

89 and Space Administration (NASA) Cryospheric Sciences Research Portal. We use the

90 yearly MO from 1979 to 2018, with a spatial resolution of ~25 km. Following the

91 method in Liang and Su (2021), we fill in the missing MO values based on surface air

92 temperature (SAT) datasets from the International Arctic Buoy Programme/Polar

93 Exchange at the Sea Surface (IABP/POLES) for 1979-2004 and the Atmospheric

94 InfraRed Sounder (AIRS) for 2005-2018. Although the missing values are not quite a

95 lot, the analysis here is more convenient if the whole research area in the LS and ESS

96 is covered.

97   The sea ice concentration (SIC) dataset, called Ocean and Sea Ice Satellite

98 Application Facility (OSI SAF), is from the European Organization for the Exploitation

99 of Meteorological Satellites (EUMETSAT) (Lavergne et al., 2019). We use the monthly

100 SIC in May from 1979 to 2018, with a resolution of 25 km. We also examine SIC dataset

101   by the NASA Team algorithm(Cavalieri et al., 1996), which shows basically the same

102   patterns in May as OSI SAF.

103   The atmospheric variables and surface energy fluxes are from the ERA5 reanalysis

104   by the European Centre for Medium-Range Weather Forecasts (ECMWF) (Hersbach et

105   al., 2020), which replaces the ERA-Interim reanalysis that ceased production in 2019.

106   The variables used in this study are monthly downward longwave radiation (DLR), net

107   longwave radiation (NLR), downward shortwave radiation (DSR), net shortwave

108   radiation (NSR), surface latent heat flux (SLHF), surface sensible heat flux (SSHF),

109   total-column water vapor (TWV), and SAT and wind fields at the 850-hPa level, for the

110   month of May from 1979 to 2018. The spatial resolution of ERA5 used in this study is

111     $0.25° \times 0.25°$, less than 30 km in the region of the Laptev Sea and East Siberian Sea.

112   Note that the four components of the surface energy balance (SEB) include NLR, NSR,

113   SLHF, and SSHF.

114

115

116 **3. Results**

117 *3.1 Distinct Melt Advance Scenarios in the Laptev Sea and East Siberian Sea*

118   Sea ice begins to melt at the surface in spring when solar radiation increases and the

119   atmosphere warms. On average, the sea ice surface in the Laptev Sea (LS) and East

120   Siberian Sea (ESS) begins to melt during May and June (Fig. 1a). Naturally, sea ice

121   melting advances northward in a given year. The range for the interannual change of

122   MO in a given place is expected to be around one month (Fig. 1b). In order to

123   demonstrate the progress of MO in different years, melt advance (MA) is defined by

124   calculating the areal percentage of an individual sea that has experienced MO at the end

125   of May (see magenta contour line in Fig. 1a). In this way, we can detect whether sea-

126   ice surface melting advances slowly or quickly in a specific year, as well as the spatial

127   patterns of the melt advance. For the seasonal prediction of summer sea ice, this metric

128   of Melt Advance is in essence similar to the average MO date, but may have advantages

129 if we can get real-time satellite MO for the region. Then, at the end of May or other

130 specific date, we can get the MA pattern which supports timely seasonal prediction.

131   Figure 1c shows the time series of MA for the LS and ESS during 1979-2018. The

132 variability is large, ranging from near zero to 100%. This implies changeable spring

133 conditions on the interannual scale. On average, MA is around 40% for each sea,

134 meaning that ~40% of the sea area has experienced sea-ice surface melting at the end

135 of May. In the context of global warming, MA has an increasing tendency in both seas

136 although this tendency is not quite significant (less than 6% per decade). This indicates

137 that we sometimes need to pay more attention to the interannual variability than to the

138 long-term linear tendency. We can also notice that relatively slow MA in the 1980s

139 contributes considerably to the overall positive tendency.

140
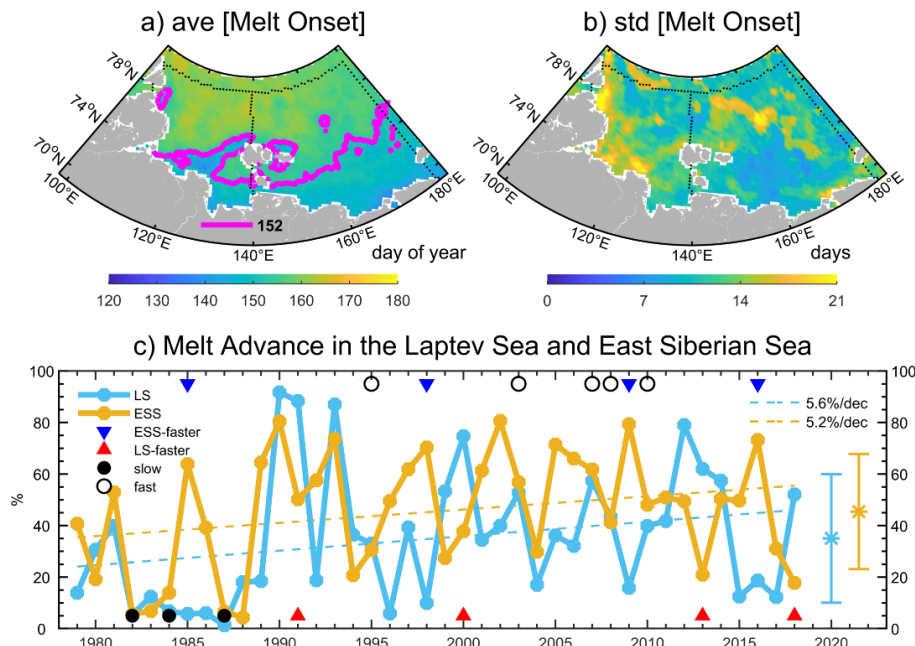
141

142 **Fig. 1.** (a, b) Climatology and standard deviation of sea ice Melt Onset, and (c) Melt
143 Advance time series in the Laptev Sea and East Siberian Sea, 1979-2018. The magenta
144 lines in panel (a) are contours of 152 (day of year), representing the end of May. The
145 areal percentage of sea ice Melt Onset earlier than 152 (day of year) is defined as Melt
146 Advance. In panel (c), only the trend of Melt Advance in the ESS is statistically
147 significant at the 90% confidence level. The average and standard deviation of the Melt
148 Advance in the LS and ESS are 35%±25% and 45%±22%, respectively. Sample years
149 (16 out of the long time-series) that fall into one of four categories are marked (see also
150 Table 1).

151

Another feature is related to the relationship of MA between the LS and ESS. In some years, MA in both the LS and ESS is slow, as in the 1980s; in other years, MA in both seas may be fast; and in other years, MA can be substantially different in the two seas. Thus, four categories of sample years are selected for further composite analysis (Table 1 and markers in Fig. 1c; MA difference between the LS and ESS is shown in Fig. S2), which represent four basic scenarios of MA in this region. Specifically, years with significantly faster MA in the ESS than in the LS ($\delta > 48\%$) are grouped as the ESS-faster-scenario, while years with significantly faster MA in the LS than in the ESS ($\delta > 33\%$) are classified as the LS-faster-scenario. The slow-scenario includes years when MA in both seas is slow (below 20%), while the fast-scenario consists of years when MA in both seas is relatively fast (between 30% and 60% at the same time). So, two pairs of contrasting categories are formed (ESS-faster-scenario vs. LS-faster-scenario, slow-scenario vs. fast-scenario). Note that to some extent the latter two scenarios represent the contrast between the 1980s and subsequent decades. Such categorization also reflects the large variability of MA in spring from the interannual perspective.

168

Category	Years	Description
ESS-faster-scenario	1985, 1998, 2009, 2016	significantly faster Melt Advance ($\delta > 48\%$) in the ESS than in the LS
LS-faster-scenario	1991, 2000, 2013, 2018	significantly faster Melt Advance ($\delta > 33\%$) in the LS than in the ESS
slow-scenario	1982, 1984, 1987	similar but slow Melt Advance ($\delta < 8\%$, but below 20%)
fast-scenario	1995, 2003, 2007, 2008, 2010	similar but fast Melt Advance ($\delta < 9\%$, but between 30% and 60%)

Table 1 List of years under different scenarios of Melt Advance.
Note: Practically, the ESS-faster-scenario and LS-faster-scenario are selected based on one standard deviation of the difference in Melt Advance between the Laptev Sea and East Siberian Sea. The slow-scenario and fast-scenario include years when Melt Advance in the two seas is quite close. All years listed here are marked in Fig. 1c.

174

175   Composite results show that the ESS-faster-scenario has substantially earlier MO,

176   i.e., faster MA in the ESS than in the LS, while the LS-faster-scenario has a somewhat

177   opposite signal (indicated by the magenta line in Fig. 2). For the slow-scenario, little

178   area in either sea has experienced MO until the end of May, indicating slow MA; for

179   the fast-scenario, nearly half of both seas has begun to experience sea-ice surface

180   melting, indicating fast MA at almost the same pace. From the surface energy balance

181   (SEB) in May, we find consistent patterns. With the zero lines of SEB as a reference,

182   the ESS-faster-scenario has relatively more positive SEB in the ESS than in the LS,

183   while the opposite is true for the LS-faster-scenario. For the slow-scenario, SEB is

184   negative over most of the two seas, while for the fast-scenario, SEB is positive in both

185   seas. This fits well with common sense. Although MA-related albedo changes may

186   amplify the SEB signals in a two-way interaction, it is fair to say that SEB in May

187   drives different patterns of MA (see individual years in Fig. S3).

188   In the next section, we investigate systematic processes under different MA

189   scenarios that involve the atmosphere, sea ice, and surface energy fluxes.

190

191
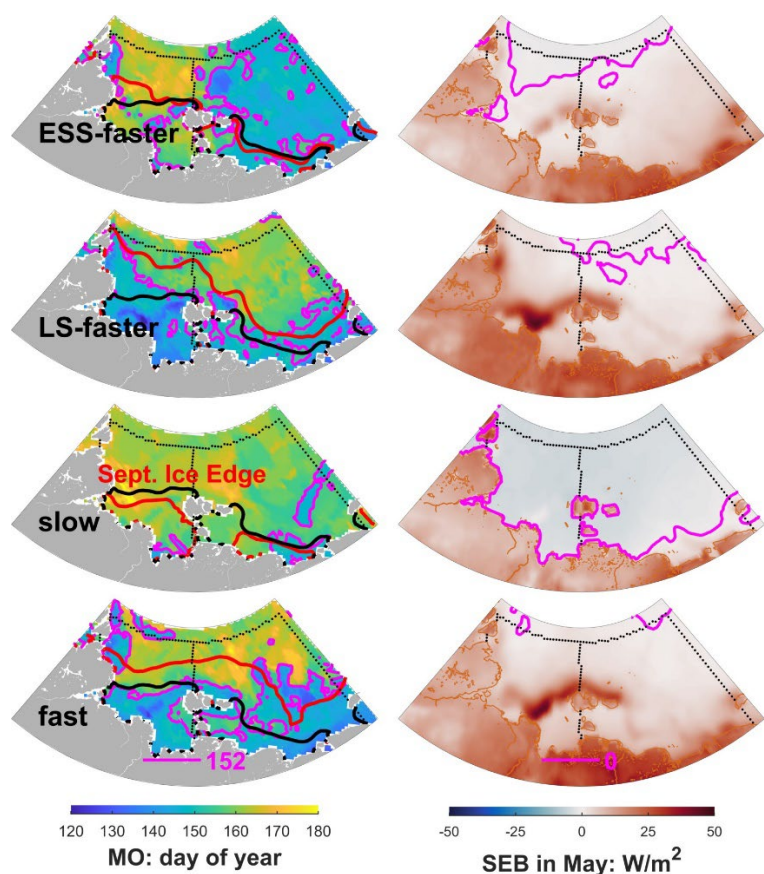
Fig. 2. Composites of MO and surface energy balance (SEB) in May for the four scenarios. The left column shows the MO patterns marked by magenta contour lines with the value of 152 (day of year) which represents the end of May. Red contour lines show the composite September ice edge, while black contour lines denote the climatological September ice edge for 1979-2018. The right column is the SEB in May, with magenta contour lines of zero. Black dots denote the boundaries of the LS and ESS.

3.2 Dynamic and Thermodynamic Processes under Different Melt Advance Scenarios

Climatologically, SEB is basically positive (~5 W/m²) across the two seas in May (see first row in Fig. S4). Among the components, it is positive net shortwave radiation (NSR) that compensates for losses from net longwave radiation (NLR), SLHF, and SSHF. This implies that on average the atmosphere receives energy from the surface through the latter three components in May. SAT is around -6°C, while sea ice almost fully covers the ocean (~90%) (see first row in Fig. 3). In the lower troposphere (850 hPa), southeasterlies blow across the region, which to some extent explains the existence of polynyas in the middle LS, i.e., regions where sea ice concentration is

210   below 75%. Note that Fig. 3 shows only selected vital variables; other relevant factors

211   can be found in Fig. S4-S7.

212
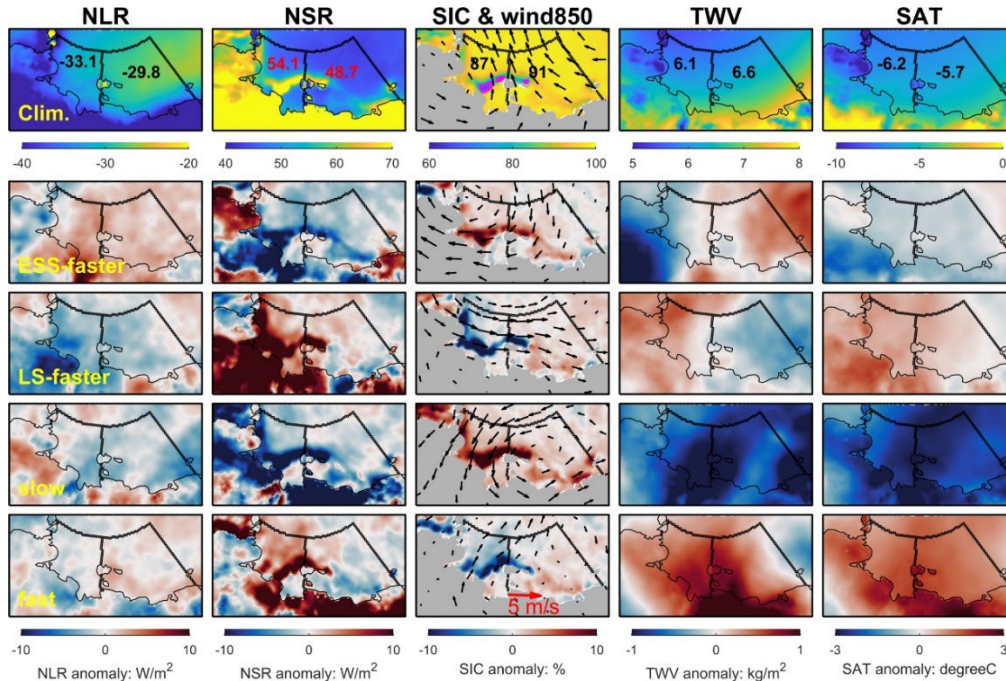
Fig. 3. Climatology (first row) and composite anomalies for the four scenarios (lower four rows) of relevant atmospheric and sea ice variables in May: NLR, NSR, SIC, winds at 850 hPa, TWV, and SAT. Numbers within the LS and ESS are the region-mean values, respectively. Note that magenta lines in the climatological SIC fields denote contours of 75% SIC values, which suggest the location of polynyas.

In the ESS-faster-scenario (see second row in Fig. 3 and blue bars in Fig. 4), prevailing northeasterlies in the lower troposphere tend to increase SIC and reduce polynya area, especially for the LS, which increases surface albedo and decreases solar radiation absorption. The northeasterlies seem to also bring slightly cool air masses to the region, and slightly moist air masses to the ESS. Given that sea ice cover is more packed, longwave radiation loss from the surface to the atmosphere is reduced, which to some extent compensates for the reduced solar radiation absorption. Due to the greater negative anomaly of solar radiation absorption in the LS, the net surface energy balance is a loss in the LS, but a gain in the ESS (Fig. S4 and S6). In addition, sea-ice surface melting is usually preconditioned by increased water vapor in the atmosphere

230 (Mortin et al., 2016). So, faster Melt Advance in the ESS is expected as TWV is

231 increased in the ESS. However, in this case, as depicted in Fig. 4, no anomaly extends

232 beyond the interannual standard deviation for the LS and ESS, suggesting a risk of over-

233 interpretation. One plausible explanation is that the normal state in this region tends to

234 resemble the ESS-faster-scenario, as indicated by Fig. 1a and the higher climatological

235 Melt Advance value in the ESS compared to the LS shown in Fig. 1c. Additionally,

236 multiple atmospheric setups may lead to the ESS-faster-scenario, highlighting the

237 considerable variability in springtime conditions. Hence, the low signal-to-noise ratio

238 is understandable. It's worth noting that the LS exhibits more notable differences,

239 consistent with its significant polynya activity.

240   For the LS-faster-scenario (see third row in Fig. 3 and red bars in Fig. 4), wind fields

241 at 850-hPa show unified westerlies over the LS and northwesterlies over the ESS, which

242 to some extent account for the reduced sea ice cover in the LS and the slightly packed

243 sea ice in the ESS. While the westerlies may not fully account for the reduced sea ice

244 in the LS, this circulation includes an offshore wind component in the western LS,

245 resulting in increased polynya opening. This includes polynyas such as the Northeast

246 Taymyr polynya, the Taymyr polynya, and the Anabar-Lena polynya (Krumpen et al.,

247 2011). So, we see a substantial increase in solar radiation absorption (beyond one

248 standard deviation) in the LS. While longwave radiation loss is somehow enhanced, the

249 net surface energy balance is still a gain for the LS and a loss for the ESS. The westerlies

250 may also bring warm and wet air masses from the North Atlantic and contribute to

251 positive anomalies of TWV and SAT in the LS, which promotes faster MA. We may

252 expect that reduced sea ice cover in the LS enables more moisture to be released from

253 the exposed ocean. However, latent heat loss as well as sensible heat loss toward

254 atmosphere in the LS weakens (Fig. S4 and S6), which suggests that warmer and

255 moister atmosphere is mainly a result of air mass transport and in turn reduces turbulent

256 heat loss from the surface.

257
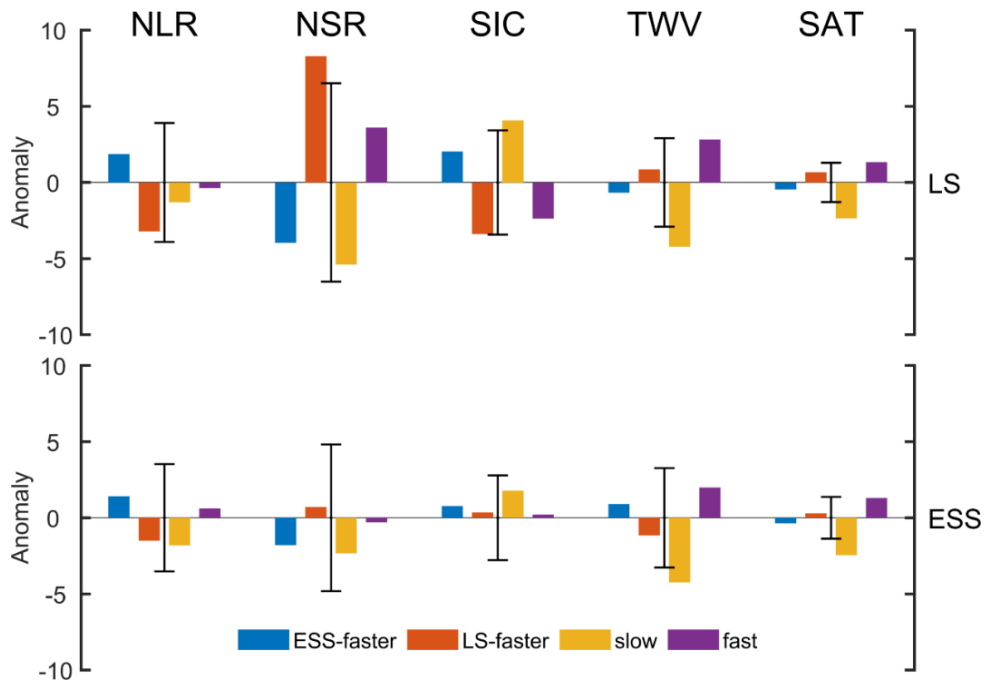
Fig. 4. Region-mean composite anomalies in the LS and ESS for the four scenarios shown in Fig. 3. The error bars denote the corresponding standard deviation for 1979-2018. The variables of NLR, NSR, SIC, TWV, and SAT have units of W/m^2, W/m^2, %, kg/m^2, and K, respectively. Here, SIC is represented by the areal percentage of sea ice cover relative to the whole sea. To facilitate viewing, TWV is scaled by a factor of 5.

For the slow-scenario (see fourth row in Fig. 3, and orange bars in Fig. 4), a cyclonic anomaly in the lower troposphere, which is centered on the ESS, pushes sea ice against the southern coast in the western half of the LS, and against the fast ice zone in the eastern half, thereby preventing polynya formation. More sea ice cover in both seas decreases solar radiation absorption. Meanwhile, this region is under the influence of cold and dry air masses (beyond one standard deviation), which induce a large loss of longwave radiation and SSHF from the surface. As a whole, we see unified surface energy deficits in the LS and ESS (beyond one standard deviation). Note that all the three sample years are from the 1980s. So, the larger sea ice cover and cooler atmosphere mainly reflect the Arctic state in the 1980s, which is a decadal phenomenon rather than interannual characteristics. We also examine the monthly snowfall under the four scenarios (Fig. S5). For this region, snowfall dominates the total precipitation in May. Especially for the slow melt advance scenario, snowfall is abnormally high, which

278   will also result in high surface albedo.

279   For the fast-scenario, with sample years after the 1980s (see last row in Fig. 3, and

280   purple bars in Fig. 4), southerlies in the lower troposphere blow mainly across the LS,

281   which drive sea ice off the coast, open the polynya and in turn increase shortwave

282   radiation absorption. At the same time, the southerlies bring warm and wet air masses

283   to this region, which substantially reduce the SSHF loss from the surface. As a result,

284   we see a positive net surface energy balance in this region and relatively fast MA.

285   The composite analysis above indicates that circulation in the lower troposphere in

286   spring in this region can be quite changeable (see individual years in Fig. S8), which

287   can have two effects: one is related to sea ice dynamics; the other involves moisture

288   and air mass advection. The former produces strong regulation of NSR due to albedo

289   changes, while the latter has everything to do with the atmospheric state, which favors

290   sea-ice surface melting when the atmosphere is warm and wet.

291   Figure 5 further shows the statistical correlation related to MA, covering years from

292   1979 to 2018. In general, we see that faster MA is accompanied by warm and wet

293   atmosphere. The related atmospheric circulation in the lower troposphere may also

294   drive reduced SIC and subsequent increased solar radiation absorption. Note that the

295   variability of SIC and NSR in the ESS is smaller than in the LS if the single outlier is

296   removed from the ESS data (see the second and third plots in the bottom row of Fig. 5).

297   Once more, this is related to the significant polynya activity observed in the LS. In

298   addition, Mortin et al. (2016) argued that on a synoptic scale, increased water vapor in

299   the atmosphere favors stronger DLR, which promotes sea-ice surface melting. Such

300   conclusion makes sense when we focus on sea ice and atmosphere above. While we

301   examine from the perspective of the whole region, including effects of the open ocean,

302   results here suggest that on the subseasonal scale net longwave radiation has little

303   connection with MA (see first column in Fig. 5). To some extent, the weak correlation

304   even shows that on the monthly scale, longwave radiation loss tends to be more when

305   SEB is more and MA is faster, which suggests some negative feedback probably related

306 to the open ocean.

307   While NSR is strong, downward shortwave radiation tends to be less (see Fig. S9),

308 which is expected from more moisture in the atmosphere. However, cloud analysis

309 based on ERA5 reanalysis doesn't suggest significant effects of clouds. Total cloud

310 cover in this region generally is larger than 90% in May and interannual anomaly is

311 relatively small (less than 5%, see Fig. S5). This indicates that from the perspective of

312 anomaly, water vapor rather than cloud cover has considerable radiation effects in the

313 springtime. Given the large uncertainty of clouds in current datasets, this remains an

314 open question.

315

316
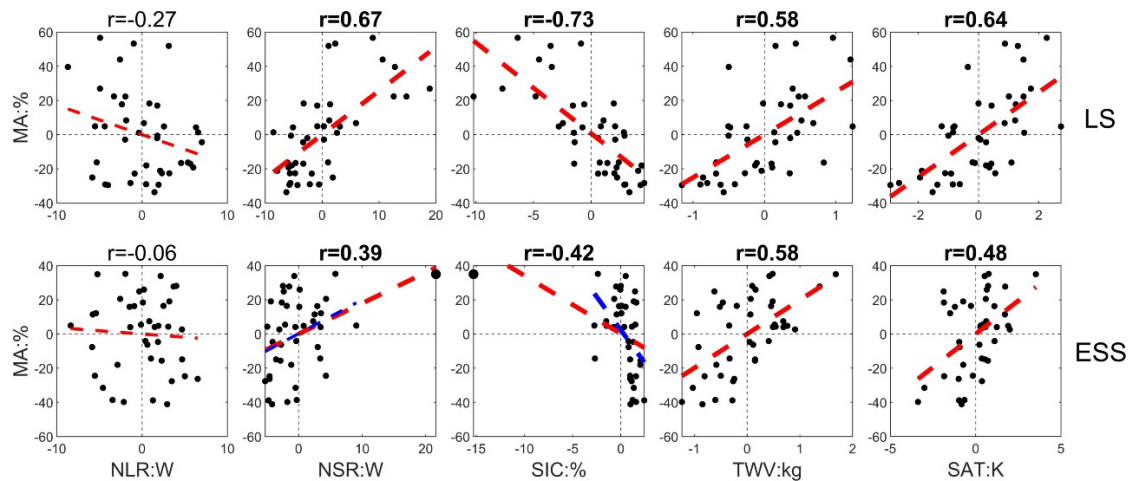
Fig. 5. Scatter plots for the period 1979-2018, illustrating the relationship between the
Melt Advance (MA) anomaly and region-mean anomalies of factors shown in Figs. 3
and 4. Thick dashed red lines represent linear fits above the 95% confidence level. Bold
titles represent correlation above the 95% confidence level. In the second and third plots
of the bottom row, thin and thick dashed blue lines respectively denote linear fits after
the removal of an outlier, identified by a larger black dot.

323

324   To what extent do different sea-ice surface melting scenarios in spring have

325 implications for sea ice cover in summer? Could we gain seasonal prediction skill based

326 on detection of sea-ice surface melting in spring? For the selected Melt Advance

327 scenarios, sea ice cover in September somewhat responds accordingly (see left column

328 in Fig. 2). In the ESS-faster-scenario, sea ice edge in September is close to climatology.

329   This echoes that the ESS-faster-scenario reflects the climatology of Melt Advance, too

330   (Fig. 1a). In the LS-faster-scenario, sea ice edge in September retreats more northward

331   in the LS part. In the slow-scenario, sea ice edge is nearer the southern coast; while in

332   the fast-scenario, sea ice edge retreats considerably in both seas. The results above

333   suggest that sea ice edge in September tends to be northward if Melt Advance at the

334   end of May is fast. Further investigation of seasonal transition of sea ice cover in the

335   four Melt Advance scenario indicates similar relationship (Fig. 6).

336
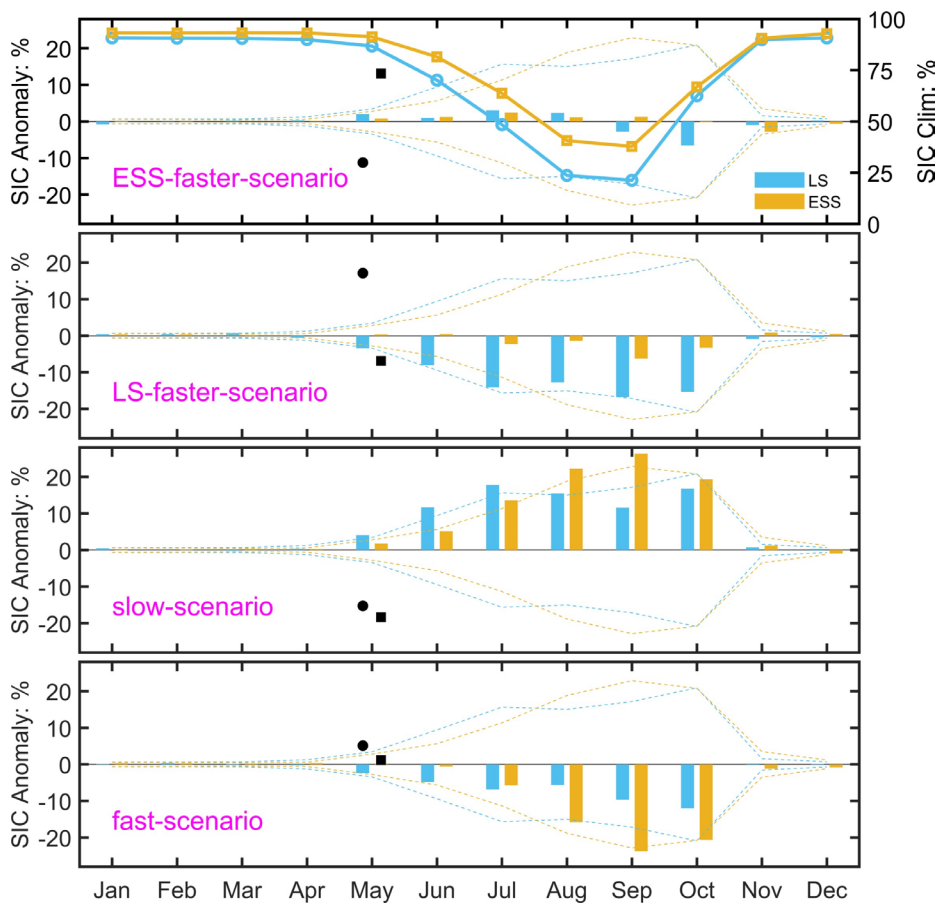
Fig. 6. Annual cycle of SIC anomaly in the four scenarios of Melt Advance. SIC is
denoted by the areal percentage of sea ice cover relative to the whole sea. Dotted lines
are the standard deviation. The mean Melt Advance in the LS and ESS is also marked
by solid dots and squares.

342

343   Figure 6 shows that in both the LS and ESS, Melt Advance in spring is significantly

344   correlated with sea ice cover in September, which is consistent with previous studies

345   utilizing Melt Onset as a predictor of summer sea ice (Petty et al., 2017; Wang et al.,

346   2011). Besides, it has similar prediction skill (statistical correlation) as average MO or

347   SIC in May. In general, the connection between springtime and summer seems to be

348   stronger in the LS than in the ESS. Given that the metric of Melt Advance can be

349   reliably defined on the same day every year (not necessarily the end of May), it has the

350   potential to be fed into the statistical or Artificial Intelligence prediction of summer sea

351   ice cover once real-time satellite detection is available. At least, it can be commonly

352   used as the average Melt Onset. Beyond this, for the prediction of summer sea ice cover,

353   the seasonal evolution from spring to summer is still a challenge as it is not fully

354   understood.

355
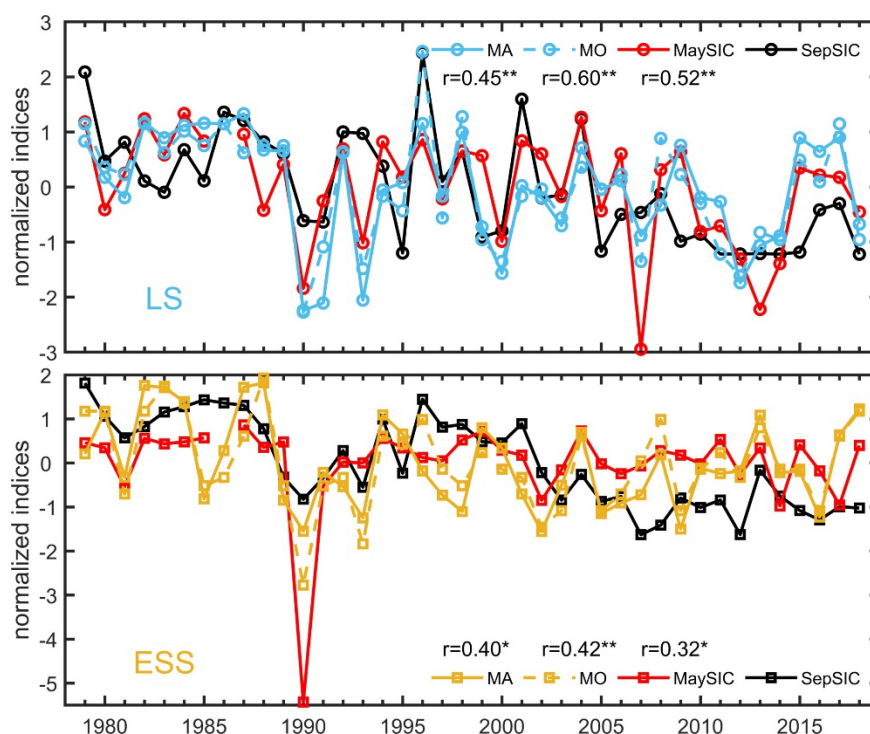
356

357   **Fig. 7.** Sea-ice surface Melt Advance, average Melt Onset, and Sea Ice Concentration
358   (SIC) in May and September in the Laptev Sea (top) and East Siberian Sea (bottom)
359   from 1979 to 2018. The May and September sea ice cover are denoted by the areal
360   percentage relative to the whole sea. All variables have been normalized. For better
361   visualization, Melt Advance is multiplied by -1. Correlation coefficients with double
362   asterisks denote 99% confidence, while those with a single asterisk denote 90%
363   confidence.

364

4. Discussion

In this study, sampling for different scenarios of sea ice Melt Advance is based on the Melt Onset dataset, which is a satellite observation product. To our knowledge, ERA5 to some extent incorporates the sea ice concentration dataset of OSI SAF, but not the Melt Onset dataset (Hersbach et al., 2020). ERA5 atmospheric reanalysis and different Melt Advance patterns can be seen as independent sources of information and their consistency should provide more confidence.

In fact, the concept of Melt Advance can be used for the whole Arctic, and can describe how sea-ice surface melting advances in spring. As mentioned above, Melt Advance can also be used as relatively independent information with reference to an atmospheric reanalysis dataset. Liang and Zhou (2023) identified three modes of Melt Onset in the LS and ESS by EOF decomposition. The positive L-mode and E-mode in their study correspond to LS-faster-scenario and ESS-faster-scenario, while the positive and negative LE-mode relate to fast-scenario and slow-scenario, respectively.

Regarding SIC anomaly in the LS and ESS, we should bear in mind that before melting the shelf areas of the LS and ESS are covered with extensive fast ice (up to 200 km wide), which is formed by April (Selyuzhenok et al., 2015). SIC in May can increase due to specific wind fields, but it probably does not consolidate against the land. Instead, the SIC anomaly is closely related to polynya development. As Fig. 3 shows, the largest SIC anomaly under the four scenarios usually occurs around the polynya region (Willmes et al., 2011).

5. Conclusions

In this study, the metric of Melt Advance (MA) is used to measure sea-ice surface melting instead of region-mean Melt Onset. MA is defined as the areal percentage of a sea in which the sea ice surface has begun to melt at the end of May, in this case the

393 Laptev Sea (LS) and East Siberian Sea (ESS). This metric has the potential to help

394 seasonally predict summer sea ice for the whole Arctic.

395   Four representative scenarios of Melt Advance in the LS and ESS are identified: the

396 ESS-faster-scenario, LS-faster-scenario, slow-scenario, and fast-scenario. Composite

397 analyses reveal that in these distinct scenarios of Melt Advance, atmospheric circulation,

398 sea ice dynamics (polynya activities), air mass advection, and surface energy fluxes are

399 related with each other. ESS-faster-scenario is associated with positive TWV anomaly

400 over the ESS and negative TWV anomaly over the LS. LS-faster-scenario and fast-

401 scenario seem to occur when polynya in the Laptev Sea opens. But the slow-scenario

402 mainly reflect the cool Arctic state in the 1980s. In addition, polynya activity in this

403 region and initial sea ice condition are also not neglectable.

404   Although sea ice Melt Advance as well as average Melt Onset and sea ice cover in

405 May are both statistically correlated with sea ice cover in September, seasonal evolution

406 can to a large extent disturb this linkage. This study suggests a need to further

407 investigate the changeable spring circulation in the lower troposphere and seasonal

408 evolution in the Arctic.

409

410

Data Availability Statement.

The sea ice MO dataset is from NASA's Cryospheric Sciences Research Portal (https://earth.gsfc.nasa.gov/cryo/data/arctic-sea-ice-melt). SAT of IABP/POLES can be accessed at https://arcticdata.io/catalog/view/doi:10.18739/A2J598, and SAT of AIRS at https://disc.gsfc.nasa.gov/datasets/AIRS3STD_006/summary. The SIC dataset of OSI SAF was downloaded from the websites below: ftp://osisaf.met.no/reprocessed/ice/conc/v2p0/ and ftp://osisaf.met.no/reprocessed/ice/conc-cont-reproc/v2p0/. The ERA5 reanalysis dataset was retrieved at https://cds.climate.copernicus.eu/cdsapp#!/search?type=dataset&keywords=((%20%22Product%20type:%20Reanalysis%22%20)). In this study, we used ERA5 monthly averaged data at single level and pressure levels.

Author Contribution

Hongjie Liang [Formal analysis; Writing original draft].

Wen Zhou [Funding acquisition; Supervision].

Competing interests

The authors declare that they have no conflict of interest.

Acknowledgments.

This work was supported by the National Natural Science Foundation of China (Grant No. 42288101, 42120104001).

REFERENCES

Bliss, A. and Anderson, M.: Snowmelt onset over Arctic sea ice from passive microwave satellite data: 1979–2012, The Cryosphere, 8, 2089-2100, 10.5194/tc-8-2089-2014, 2014.

Budyko, M. I.: The effect of solar radiation variations on the climate of the Earth, Tellus, 21, 611-619, 10.1111/j.2153-3490.1969.tb00466.x, 1969.

Cavalieri, D., Parkinson, C., Gloersen, P., and Zwally, H.: Sea ice concentrations from Nimbus-7 SMMR and DMSP SSM/I passive microwave data, National Snow and Ice Data Center, Boulder, Colorado, USA, 10.5067/8GQ8LZQVL0VL, 1996.

Cohen, J., Screen, J. A., Furtado, J. C., Barlow, M., Whittleston, D., Coumou, D.,

446   Francis, J., Dethloff, K., Entekhabi, D., Overland, J., and Jones, J.: Recent Arctic
447   amplification and extreme mid-latitude weather, Nature Geoscience, 7, 627-637,
448   10.1038/ngeo2234, 2014.
449   Crawford, A. D., Horvath, S., Stroeve, J., Balaji, R., and Serreze, M. C.: Modulation of
450   Sea Ice Melt Onset and Retreat in the Laptev Sea by the Timing of Snow Retreat
451   in the West Siberian Plain, Journal of Geophysical Research: Atmospheres, 123,
452   8691-8707, 10.1029/2018jd028697, 2018.
453   Drobot, S. D. and Anderson, M. R.: An improved method for determining snowmelt
454   onset dates over Arctic sea ice using scanning multichannel microwave radiometer
455   and Special Sensor Microwave/Imager data, Journal of Geophysical Research:
456   Atmospheres, 106, 24033-24049, 10.1029/2000JD000171, 2001.
457   Francis, J. A. and Vavrus, S. J.: Evidence for a wavier jet stream in response to rapid
458   Arctic warming, Environmental Research Letters, 10, 10.1088/1748-
459   9326/10/1/014005, 2015.
460   Hersbach, H., Bell, B., Berrisford, P., Hirahara, S., Horányi, A., Muñoz‐Sabater, J.,
461   Nicolas, J., Peubey, C., Radu, R., Schepers, D., Simmons, A., Soci, C., Abdalla,
462   S., Abellan, X., Balsamo, G., Bechtold, P., Biavati, G., Bidlot, J., Bonavita, M.,
463   Chiara, G., Dahlgren, P., Dee, D., Diamantakis, M., Dragani, R., Flemming, J.,
464   Forbes, R., Fuentes, M., Geer, A., Haimberger, L., Healy, S., Hogan, R. J., Hólm,
465   E., Janisková, M., Keeley, S., Laloyaux, P., Lopez, P., Lupu, C., Radnoti, G.,
466   Rosnay, P., Rozum, I., Vamborg, F., Villaume, S., and Thépaut, J. N.: The ERA5
467   global reanalysis, Quarterly Journal of the Royal Meteorological Society, 146,
468   1999-2049, 10.1002/qj.3803, 2020.
469   Horvath, S., Stroeve, J., Rajagopalan, B., and Jahn, A.: Arctic sea ice melt onset favored
470   by an atmospheric pressure pattern reminiscent of the North American-Eurasian
471   Arctic pattern, Climate Dynamics, 57, 1771-1787, 10.1007/s00382-021-05776-y,
472   2021.
473   Kashiwase, H., Ohshima, K. I., Nihashi, S., and Eicken, H.: Evidence for ice-ocean
474   albedo feedback in the Arctic Ocean shifting to a seasonal ice zone, Sci Rep, 7,
475   8170, 10.1038/s41598-017-08467-z, 2017.
476   Krumpen, T., Hölemann, J. A., Willmes, S., Morales Maqueda, M. A., Busche, T.,
477   Dmitrenko, I. A., Gerdes, R., Haas, C., Heinemann, G., Hendricks, S., Kassens,
478   H., Rabenstein, L., and Schröder, D.: Sea ice production and water mass
479   modification in the eastern Laptev Sea, Journal of Geophysical Research, 116,
480   10.1029/2010jc006545, 2011.
481   Lavergne, T., Sørensen, A. M., Kern, S., Tonboe, R., Notz, D., Aaboe, S., Bell, L.,
482   Dybkjær, G., Eastwood, S., Gabarro, C., Heygster, G., Killie, M. A., Brandt
483   Kreiner, M., Lavelle, J., Saldo, R., Sandven, S., and Pedersen, L. T.: Version 2 of
484   the EUMETSAT OSI SAF and ESA CCI sea-ice concentration climate data
485   records, The Cryosphere, 13, 49-78, 10.5194/tc-13-49-2019, 2019.
486   Lei, R., Cheng, B., Hoppmann, M., Zhang, F., Zuo, G., Hutchings, J. K., Lin, L., Lan,
487   M., Wang, H., Regnery, J., Krumpen, T., Haapala, J., Rabe, B., Perovich, D. K.,

and Nicolaus, M.: Seasonality and timing of sea ice mass balance and heat fluxes in the Arctic transpolar drift during 2019–2020, Elementa: Science of the Anthropocene, 10, 10.1525/elementa.2021.000089, 2022.

Liang, H. and Su, J.: Variability in Sea Ice Melt Onset in the Arctic Northeast Passage: Seesaw of the Laptev Sea and the East Siberian Sea, Journal of Geophysical Research: Oceans, 126, e2020JC016985, 10.1029/2020JC016985, 2021.

Liang, H. and Zhou, W.: Arctic Sea Ice Melt Onset in the Laptev Sea and East Siberian Sea in Association with the Arctic Oscillation and Barents Oscillation, Journal of Climate, 36, 6363-6373, 10.1175/jcli-d-22-0791.1, 2023.

Markus, T., Stroeve, J. C., and Miller, J.: Recent changes in Arctic sea ice melt onset, freezeup, and melt season length, Journal of Geophysical Research (Oceans), 114, C12024, 10.1029/2009jc005436, 2009.

Mortin, J., Svensson, G., Graversen, R. G., Kapsch, M.-L., Stroeve, J. C., and Boisvert, L. N.: Melt onset over Arctic sea ice controlled by atmospheric moisture transport, Geophysical Research Letters, 43, 6636-6642, 10.1002/2016GL069330, 2016.

Petty, A. A., Kurtz, N. T., Kwok, R., Markus, T., and Neumann, T. A.: Winter Arctic Sea Ice Thickness From ICESat‐2 Freeboards, Journal of Geophysical Research: Oceans, 125, 10.1029/2019jc015764, 2020.

Petty, A. A., Schröder, D., Stroeve, J. C., Markus, T., Miller, J., Kurtz, N. T., Feltham, D. L., and Flocco, D.: Skillful spring forecasts of September Arctic sea ice extent using passive microwave sea ice observations, Earth's Future, 5, 254-263, 10.1002/2016ef000495, 2017.

Screen, J. A. and Simmonds, I.: The central role of diminishing sea ice in recent Arctic temperature amplification, Nature, 464, 1334-1337, 10.1038/nature09051, 2010.

Sellers, W. D.: A Global Climatic Model Based on the Energy Balance of the Earth-Atmosphere System, Journal of Applied Meteorology and Climatology, 8, 392-400, 10.1175/1520-0450(1969)008<0392:agcmbo>2.0.co;2, 1969.

Selyuzhenok, V., Krumpen, T., Mahoney, A., Janout, M., and Gerdes, R.: Seasonal and interannual variability of fast ice extent in the southeastern Laptev Sea between 1999 and 2013, Journal of Geophysical Research: Oceans, 120, 7791-7806, 10.1002/2015jc011135, 2015.

Serreze, M. C., Barrett, A. P., Stroeve, J. C., Kindig, D. N., and Holland, M. M.: The emergence of surface-based Arctic amplification, The Cryosphere, 3, 11-19, 10.5194/tc-3-11-2009, 2009.

Skeie, P.: Meridional flow variability over the Nordic Seas in the Arctic oscillation framework, Geophysical Research Letters, 27, 2569-2572, 10.1029/2000gl011529, 2000.

Stroeve, J. and Notz, D.: Changing state of Arctic sea ice across all seasons, Environmental Research Letters, 13, 103001, 10.1088/1748-9326/aade56, 2018.

Stroeve, J. C., Markus, T., Boisvert, L., Miller, J., and Barrett, A.: Changes in Arctic melt season and implications for sea ice loss, Geophysical Research Letters, 41, 1216-1225, 10.1002/2013gl058951, 2014.

530 Taylor, P. C., Boeke, R. C., Boisvert, L. N., Feldl, N., Henry, M., Huang, Y., Langen, P.
531   L., Liu, W., Pithan, F., Sejas, S. A., and Tan, I.: Process Drivers, Inter-Model
532   Spread, and the Path Forward: A Review of Amplified Arctic Warming, Frontiers
533   in Earth Science, 9, 10.3389/feart.2021.758361, 2022.
534 Wang, L., Wolken, G. J., Sharp, M. J., Howell, S. E. L., Derksen, C., Brown, R. D.,
535   Markus, T., and Cole, J.: Integrated pan-Arctic melt onset detection from satellite
536   active and passive microwave measurements, 2000-2009, Journal of Geophysical
537   Research: Atmospheres, 116, 10.1029/2011jd016256, 2011.
538 Willmes, S., Adams, S., Schröder, D., and Heinemann, G.: Spatio-temporal variability
539   of polynya dynamics and ice production in the Laptev Sea between the winters of
540   1979/80 and 2007/08, Polar Research, 30, 10.3402/polar.v30i0.5971, 2011.
541